Published in final edited form as:
Mol Neurobiol. 2014 February ; 49(1): 547–562. doi:10.1007/s12035-013-8539-y.

Intracerebroventricular streptozotocin exacerbates Alzheimer-like changes of 3xTg-AD mice[1]

Yanxing Chen[a,b,c,2], **Zhihou Liang**[c,2], **Zhu Tian**[a,d], **Julie Blanchard**[a], **Chun-ling Dai**[a], **Sonia Chalbot**[a], **Khalid Iqbal**[a], **Fei Liu**[a], and **Cheng-Xin Gong**[a,*]

[a]Department of Neurochemistry, Inge Grundke-Iqbal Research Floor, New York State Institute for Basic Research in Developmental Disabilities, Staten Island, New York 10314, USA

[b]Department of Neurology, the Second Affiliated Hospital, School of Medicine, Zhejiang University, Hangzhou, 310009, China

[c]Department of Neurology, Union Hospital, Tongji Medical College, Huazhong University of Science & Technology, Wuhan, Hubei 430022, China

[d]Department of Neurology, The First Hospital of Jilin University, Xinmin Street, Changchun, Jilin 130021, China

Abstract

Alzheimer's disease (AD) involves several possible molecular mechanisms, including impaired brain insulin signaling and glucose metabolism. To investigate the role of metabolic insults in AD, we injected streptozotocin (STZ), a diabetogenic compound if used in the periphery, into the lateral ventricle of the 6-month old 3xTg-AD mice and studied the cognitive function as well as AD-like brain abnormalities, such as tau phosphorylation and Aβ accumulation, 3–6 weeks later. We found that STZ exacerbated impairment of short-term and spatial reference memory in 3xTg-AD mice. We also observed an increase of tau hyperphosphorylation and neuroinflammation, a disturbance of brain insulin signaling, and a decrease of synaptic plasticity and amyloid β peptides in the brain after STZ treatment. The expression of 20 AD-related genes, including those involved in the processing of amyloid precursor protein, cytoskeleton, glucose metabolism, insulin signaling, synaptic function, protein kinases and apoptosis, was altered, suggesting that STZ disturbs multiple metabolic and cell signaling pathways in the brain. These findings provide experimental evidence of the role of metabolic insult in AD.

Keywords

Streptozotocin; 3xTg-AD mice; Cognitive deficits; Tau phosphorylation; Amyloid-β; Synaptic proteins; Neuroinflammation; Insulin signaling

[1]This paper is dedicated to late Inge Grundke-Iqbal, Ph.D., who made seminal contributions to our understanding of neurofibrillary degeneration in Alzheimer's disease.

[*]Corresponding author at: Department of Neurochemistry, New York State Institute for Basic Research in Developmental Disabilities, 1050 Forest Hill Road, Staten Island, NY 10314-6399, USA. Tel.: + 1 718 494 5248; Fax: + 1 718 494 1080; chengxin.gong@csi.cuny.edu.

[2]These authors contributed equally to this work.

Competing Interests The authors declare that they have no competing interests.

Introduction

Alzheimer's disease (AD) is the leading cause of dementia and is characterized by progressive loss of memory and other cognitive functions. The histopathological hallmarks of AD are extracellular amyloid-β (Aβ) plaques and intracellular neurofibrillary tangles (NFTs). Most of AD cases are sporadic, which are multifactorial and involve several different molecular mechanisms and etiological factors [1,2].

One common early brain abnormality in AD is an impairment of brain glucose uptake/metabolism, which occurs many years before the first symptoms appear [3–6], suggesting that the impaired glucose uptake/metabolism could be a cause of neurodegeneration or be mechanistically involved in AD. The impairment of brain glucose metabolism correlates well with the clinical symptoms of AD [7,8]. Our recent studies that demonstrated decreased insulin signaling and glucose transporters in AD brain [9–11] have provided a potential cause for the impaired brain glucose uptake/metabolism in this disease.

To investigate the role of disturbed brain insulin signaling and impaired brain glucose uptake/metabolism in AD, we injected streptozotocin (STZ), a diabetogenic compound that causes pancreatic β cell death and insulin resistance when administered peripherally, into the lateral ventricle of 3xTg-AD mice and studied the effects of intracerebroventricular (icv) STZ on cognitive functions, as well as tau phosphorylation, Aβ accumulation, and other related abnormalities in the mouse brains. It has been reported that the central administration of STZ causes dysregulated brain insulin signaling [12–14] and abnormalities in cerebral glucose utilization/metabolism accompanied by an energy deficit [15,16]. The 3xTg-AD mice harbor three mutant human transgenes—$PS1_{M146V}APP_{Swe}$ and tau_{P301L} [17–19]—and develop amyloid plaques, NFTs, and cognitive deficits in an age-dependent manner [20–22]. This AD mouse model has been well-characterized and widely used in the AD field.

In the preset study, we found that administration of STZ into the brain exacerbated cognitive deficits in the 3xTg-AD mice, which were accompanied by an increase of tau hyperphosphorylation and neuroinflammation, a disturbance of insulin signaling, a decrease of synaptic plasticity and amyloid β peptides, and alterations of the expression of 20 AD-related genes in the brain.

Materials and Methods

Antibodies and Reagents

Primary antibodies used in this study are listed in Table 1. Peroxidase-conjugated antimouse and anti-rabbit IgG were obtained from Jackson ImmunoResearch Laboratories (West Grove, PA, USA). The enhanced chemiluminescence (ECL) kit was from Pierce (Rockford, IL, USA). ABC staining system was from Santa Cruz Biotechnology (CA, USA). Human $Aβ_{1–40}$ and $Aβ_{1–42}$ ELISA kits were from Invitrogen (Carlsbad, CA, USA). RT^2 Profiler PCR Array system was from Qiagen (Valencia, CA). Other chemicals were from Sigma (St. Louis, MO, USA).

Animals

The homozygous 3xTg-AD mouse harboring $PS1_{M146V}$, APP_{Swe} and tau_{P301L} transgenes and the wild type (WT) control mouse (a hybrid of 129/Sv and C57BL/6 mice) were initially obtained from F.M. LaFerla through the Jackson Laboratory (New Harbor, 124 ME, USA). Mice were housed (4~5 animals per cage) with a 12/12 h light/dark cycle and with ad libitum access to food and water. The housing, breeding, and animal experiments were in accordance with the approved protocol from our Institutional Animal Care and Use

Committee, according to the PHS Policy on Human Care and Use of Laboratory animals (revised March 15, 2010).

The 3xTg-STZ mice were produced by stereotaxic injection of STZ [2–deoxy–2–(3–(methyl–3–nitrosoureido)-D-glucopyranose), from Sigma-Aldrich, St. Louis, MO] into the left lateral ventricle of the 3xTg-AD mice (female, 6 months old). Briefly, mice were first anesthetized using 2.5% avertin (2,2,2-tribromoethanol, Sigma-Aldrich), a commonly used anesthetic for mice which produce a wide anesthetic window, and then restrained onto a stereotaxic apparatus. The bregma coordinates used for injection were: −1.0 mm lateral, −0.3 mm posterior, and −2.5 mm below. Each mouse received a single icv injection of 3.0 mg/kg STZ in 3.0 μl 0.9% saline into the left ventricle of the brain. The control WT mice and the control 3xTg-AD mice (all female, 6 months old) were treated identically but with vehicle (0.9% saline) only. Twenty one days after icv injection, the mice were subjected to a battery of behavioral tests which lasted for 3 weeks (Fig. 1A). Finally, the mice were sacrificed by decapitation, and the brains were removed immediately. The hippocampus, cerebral cortex, subcortical structures, cerebellum and brain stem were dissected, flash frozen in dry ice, and stored at −80°C for biochemical analyses at a later date. Some brains were fixed with 4% paraformaldehyde in 0.1 M PBS, followed by cryoprotection in 30% sucrose. Sagittal sections (40-μm thick) were cut using a freezing sliding microtome. The sections were stored in glycol anti-freeze solution (ethylene glycol, glycerol, and 0.1 M PBS in 3:3:4 ratio) at −20°C until immunohistochemical staining.

In this study, we included 18 3xTg-saline mice, 26 3xTg-STZ mice, and 18 WT-saline mice for behavioral tests, and 7–9 mice per group for biochemical and immunohistochemical analyses. Female 3xTg-AD mice aged 6 months old were used in this study because these mice start to show AD-related brain abnormalities (but not NFTs or amyloid plaques) and cognitive impairment at this age [20–22], which would give a good window to investigate the effects of STZ, and because young female 3xTg-AD mice develop behavioral deficits faster than the male mice [21], which would facilitate our study.

Elevated plus maze

Elevated plus maze was used to evaluate anxiety/emotionality of the mice. It consisted of four arms (30×5 cm) connected by a common 5×5 cm center area. Two opposite facing arms were open (OA), whereas the other two facing arms were enclosed by 20 cm high walls (CA). The entire plus-maze was elevated on a pedestal to a height of 82 cm above floor level in a separated room from the investigator. The mouse was placed onto the central area facing an open arm and allowed to explore the maze for a single 8 min session. Between each session, any feces were cleared from the maze, and the maze floor was cleaned with 70% alcohol to remove any urine or scent cues. The number of CA entries, OA entries, and the amount of time spent in CA and OA were recorded by a video tracking system (ANY-Maze version 4.5 software, Stoelting Company, Wood Dale, IL, USA).

Open field

Anxiety and exploratory activities were evaluated by allowing mice to freely explore an open field arena for 15 min. The testing apparatus was a classic open field (i.e. a PVC square arena, 50 × 50 cm, with walls 40 cm high), surmounted by a video camera connected to a computer. Each mouse was placed individually in the arena and the performance was monitored and the time spent in the center and peripheral area and the distance traveled in the arena were automatically recorded by a video tracking system (ANY-Maze version 4.5 software, Stoelting Co.).

One-trial object recognition task

Mice were tested for one-trial object recognition based on the innate tendency of rodents to differentially explore novel objects over familiar ones in an open field arena, using a procedure modified from a previous description [23]. The procedure consisted of three different phases: a habituation phase, a sample phase, and a test phase. Following initial exposure, four additional 10-min daily habituation sessions were introduced to mice for becoming familiar with the apparatus and the surrounding environment. On the fifth day, every mouse was first submitted to the sample phase of which two identical objects were placed in a symmetric position from the center of the arena and was allowed to freely explore the objects for 5 min. After a 15-min delay during which the mouse was returned to its home cage, the animal was reintroduced in the arena to perform the test phase. The mouse was then exposed to two objects for another 5 min: a familiar object (previously presented during the sample phase) and a novel object, placed at the same location as during the sample phase. Data collection was performed using a video tracking system (ANY-Maze version 4.5 software, Stoelting Co.). Object discrimination was evaluated by the index: [(time spent exploring the new object)/(time spent exploring both old and new objects)] during the test phase.

Accelerating Rotarod test

Motor coordination and balance of mice were assessed by using a Rotarod test. Test on accelerating Rotarod was conducted by giving each mouse two sessions of three trials on a rotating cylinder. The speed increased steadily from 4 to 40 rpm over a 5-min period. The latency to fall off the Rotarod was calculated. Inter-trial intervals were 10–15 min for each mouse.

Morris water maze

Spatial reference learning and memory were evaluated in a water maze adapted from that previously described by Morris and collaborators [24]. The test was performed in a white pool of 180 cm in diameter filled with water tinted with non-toxic white paint and maintained at room temperature (21 ± 2°C). During training, a platform (14 cm in diameter) was submerged 1 cm below water surface. All mice were given four trials per day for four consecutive days. The starting position was randomized among four quadrants of the pool. For each trial, the animal was given 90 sec to locate the hidden platform. If a mouse failed to find the platform within 90 sec, it was gently guided to it. At the end of each trial, the mouse was left on the platform for 20 sec, then dried and returned to its home cage until the next trial. Probe trial was given 24 h after the last day of training. During the probe trial, mice were allowed to swim in the pool without the escape platform for 60 sec. The latency to reach the platform site (sec), swim distance (cm), and swim speed (cm/sec) were recorded using an automated tracking system (Smart video tracking system, Panlab, Harvard Apparatus).

Western Blot Analysis

The hippocampi of the mouse brains were homogenized in pre-chilled 50 mM tris-HCl buffer (pH 7.4) containing an O-GlcNAc transferase inhibitor (20 μM UDP), an O-GlcNAcase inhibitor (50 mM N-acetylglucosamine), protein phosphatase inhibitors (2 mM $Na_3VO_4$50 mM NaF and 20 mM Glycero-P) and protease inhibitors (2.0 mM EGTA, 0.5 mM AEBSF, 10 μg/ml aprotinin, 10 μg/ml leupeptin and 4 μg/ml pepstatin A). Protein concentrations of the homogenates were determined by using modified Lowry method [25]. The samples were resolved in 10% or 12.5% SDS-PAGE and electrotransferred onto Immobilon-P membrane (Millipore, Bedford, MA). The blots were then probed with primary antibody and developed with the corresponding horseradish peroxidase–conjugated

secondary antibody and enhanced chemiluminescence kit (Pierce, Rockford, IL). Densitometric quantification of protein bands in Western blots were analyzed by using the TINA software (Raytest IsotopenmeBgerate GmbH, Straubenhardt, Germany).

Immunohistochemical staining

Floating sections were incubated for 30 min with 0.3% H_2O_2 and 0.3% Triton X-100 for 15 min at room temperature, washed in PBS, and blocked in a solution containing 5% normal goat serum and 0.1% Triton X-100 for 30 min. Sections were then incubated overnight at 4°C with primary antibody before applying biotinylated secondary antibody and then avidin/biotinylated horseradish peroxidase (Santa Cruz Biotechnology). The sections were stained with peroxidase substrate and then mounted on microscope slides (Brain Research Laboratories, Newton, MA, USA), dehydrated, and covered with coverslips.

Aβ measurements

Hippocampal levels of both total $A\beta_{1–40}$ and $A\beta_{1–42}$ were measured by ELISA kits from Invitrogen (Carlsbad, CA, USA) using specific anti-human Aβ antibodies. Briefly, the right hippocampi were homogenized in 8×volume of 5.0 M guanidine HCl in 50 mM Tris-HCl (pH 7.6) and incubated for 4 h at room temperature. The homogenates were then diluted with the cold reaction buffer prepared according to the manufacturer's instruction and centrifuged at 16,000 *g* at 4°C for 20 min. The resulting supernatants were further diluted in standard diluent buffer in order to reach a final 0.1M guanidine concentration. Both $A\beta_{1–40}$ and $A\beta_{1–42}$ levels were subsequently measured according to the manufacturer's instructions.

RT^2 Profiler PCR Array

The expression profiles of 84 AD-related genes in the mouse brain were analyzed by using a custom-designed RT^2 Profiler PCR Array system from Qiagen (Valencia, CA, USA) according to manufacturer's instruction. Briefly, total RNA was isolated from the cerebral cortical and hippocampal samples using the RNeasy Mini kit (Qiagen). Only RNA samples with A260/A230 ratios greater than 1.8, A260/280 ratios greater than 1.9, and 28S/18S ratios around 2 in agarose gel electrophoresis were used for further study. Total RNA (1 μg) was subjected to reverse transcription reaction using the RT^2 First-Strand Kit (Qiagen). Then, the first-strand cDNA synthesis reaction mixture was used for real-time PCR using RT^2 SYBR Green ROX qPCR Master Mix (Qiagen) and the custom-made 96-well PCR arrays in a Stratagene Mx3000p PCR detection system.

Statistical analysis

For biochemical analyses, data were analyzed by one-way ANOVA or unpaired two-tailed *t* tests, followed by Tukey's post hoc tests, using GraphPad. For body weight measurement, fall latency on Rotarod, distance traveled in the open field and distance traveled during water maze training, repeated measures two-way ANOVA with Fisher's LSD post hoc tests were performed using STATVIEW. For the rest behavioral measurements, one-way ANOVA with Fisher's LSD post hoc tests were performed. Data generated from RT^2 Profiler PCR Array were analyzed using Qiagen's web-based PCR array data analysis system (http://pcrdataanalysis.sabiosciences.com/pcr/arrayanalysis.php), which is based on $\Delta\Delta C_t$ comparative method and unpaired two-tailed student *t* test. All data are presented as means ± SEM, and $p<0.05$ was considered statistically significant.

Results

STZ exacerbates cognitive deficits in 3xTg-AD mice

During the study, we monitored the general condition daily and weighed the mice once a week. We found that the icv STZ killed 31% of the 3xTg-AD mice (Fig. 1B). Seven out of 29 3xTg-AD mice died within the first week after icv STZ injection, and 2 mice died in the following 2 weeks. In contrast, no WT or 3xTg-AD mice that received saline injection died. All mice experienced some loss of weight during the first week after icv injection (Fig. 1C). However, the body weights of the 3xTg-AD mice with saline injection (3xTg-saline mice), but not those with icv STZ (3xTg-STZ mice), were recovered.

Before analyzing cognitive functions, we first evaluated general behavior of the mice. Rotarod tests indicated that the 3xTg-AD mice had a much better performance, indicating a better motor coordination and balance, than the WT mice (Fig. 1D), which is consistent with previous studies [26]. Treatment of the 3xTg-AD mice with STZ slightly impaired their Rotarod performance. We also measured the spontaneous locomotor and exploratory activity of the mice in the open field test. We found that the 3xTg-STZ mice spent less time in the central area of the open field arena and traveled a longer distance than the 3xTg-saline mice (Fig. 1E, F). These results indicated that icv injection of STZ caused a higher level of anxiety in the 3xTg-AD mice. Consistently, the 3xTg-STZ mice spent less time in the open arms of the elevated plus maze (Fig. 1G), which is the most widely used test for measuring the anxiety-like behavior in rodents [27] based on animal's unconditional response to a potentially dangerous environment. Fig. 1G also indicates that icv injection of STZ aggravated the anxiety level of the 3xTg-AD mice.

To examine the short-term memory that depends on the entorhinal cortex, hippocampus, and frontal cortex [28–30], we conducted one-trial object recognition test with 15 min interval between the sample phase and the test phase. We found that all mice explored the two identical objects equally during the sample phase (Fig. 2A). As expected, we observed that the 3xTg-saline mice spent less time exploring the novel object than the WT-saline mice, as shown by a decreased discrimination index (Fig. 2B), indicating the short-term memory impairment of the 3xTg-AD mice. The 3xTg-STZ mice had an even smaller discrimination index than the 3xTg-saline mice, indicating that STZ exacerbates the short-term memory impairment in 3xTg-AD mice.

The spatial reference learning and memory of the mice was evaluated using Morris water maze test. We found that all mice were able to learn the platform location during the training period, as evidenced by a decrease in distance traveled (Fig. 2C) and in latency (data not shown) to locate the submerged platform. However, the learning curves indicate that the 3xTgsaline mice traveled a longer distance and spent a longer time (data not shown) than the WT-saline mice to find the platform (Fig. 2C), suggesting an impairment of the 3xTg-AD mice to encode and remember the spatial coordinates of the platform within the environment. STZ injection exacerbated this impairment. Retrieval of spatial memory was more specifically analyzed with the probe trial performed 24 hrs after the last training trial. Memory performance was determined by the number of the former platform site crossings, percentage of time spent at the platform site, and the percentage of time/distance animals spent/traveled in the target quadrant. We found that the 3xTg-saline mice crossed the former platform site much less and spent much less time in the platform site than the WT-saline mice, and the 3xTg-STZ mice made the least number of crossing and spent the least time (Fig. 2D, E). These results indicated that STZ exacerbates the impairments of spatial reference learning and memory of the 3xTg-AD mice. The 3xTg-STZ mice also showed a slightly lower swim speed than the WT-saline and the 3xTg-saline mice (Fig. 2F).

STZ increases tau phosphorylation in 3xTg-AD mice

Mainly as the consequence of overexpression of $tau_{P301L}$the 3xTg-AD mice develop hyperphosphorylation and aggregation of tau and the formation of NFTs in a time-dependent manner. To determine whether the icv injection of STZ worsens tau pathology, we studied tau phosphorylation in the 3xTg-AD mouse brains. As expected, we found four-fold more total tau protein in the hippocampus of the 3xTg-AD mice as compared to the control WT mice, as detected by polyclonal tau antibody R134d (Fig. 3A, 3B), which recognizes both human and murine tau in a phosphorylation-independent manner. When the levels of tau phosphorylated at various individual phosphorylation sites were determined by a battery of phosphorylation-dependent and site-specific antibodies, we found marked increases in the levels of phosphorylated tau in the 3xTg-AD hippocampus (Fig. 3B). Furthermore, we found that icv STZ treatment of the 3xTg-AD mice further increased the level of tau phosphorylated at Ser199/202, Ser262/356 (12E8 sites) and Ser422 (Fig. 3A, 3B), as well as the net phosphorylation of tau at these sites, the latter of which was calculated after normalization with the total tau level (Fig. 3C). Immunohistochemically, the increase in the phosphorylated tau was seen both in the hippocampus and the cerebral cortex, and STZ treatment exacerbated tau pathology in these brain areas, especially in the CA1 sector of the hippocampus and the dentate gyrus (Fig. 3D). These results indicate that STZ treatment exacerbates tau phosphorylation at some AD-relevant hyperphosphorylation sites in the 3xTg-AD mice. Because the 3xTg-AD mice do not develop NFTs in the brains at this age [21,22], we did not investigate the insoluble fraction of Tau.

STZ alters Aβ level in 3xTg-AD mice

We investigated the effects of icv STZ on Aβ and APP levels in the hippocampus of the 3xTg-AD mice. We found that the levels of both total human $A\beta_{1–42}$ and $A\beta_{1–40}$as determined by ELISA, were lower in the hippocampus of the 3xTg-STZ mice than the 3xTg-saline mice, although the decrease in $A\beta_{1–42}$ did not reach statistical significance (Fig. 4A, B). The STZ treatment reduced the $A\beta_{1–40}$ level by 42%. However, the ratio of $A\beta_{1–42}$/ $A\beta_{1–40}$ was not altered by STZ injection (Fig. 4C). Because the 3xTg-AD mice do not develop amyloid plaques in the brains until they reach the age of 18 months [22], we could not investigate amyloid plaque pathology in this study. To elucidate whether the decrease of Aβ peptides with STZ treatment results from altered APP expression, we determined the level of APP by Western blots with antibody 6E10 and found that STZ did not significantly affect the APP level in the hippocampus of the 3xTg-AD mice (Fig. 4D, E).

STZ alters synaptic proteins in 3xTg-AD mice

Synaptic plasticity is regulated at the pre-synaptic site by changing the release of neurotransmitter molecules and at the post-synaptic site by changing the number, types, or properties of neurotransmitter receptors and their interactions with post-synaptic scaffold proteins. Therefore, we studied alterations of pre- and post-synaptic proteins in the mouse hippocampus, including synaptophysin (Syp), a pre-synaptic marker, and postsynaptic density 95 (PSD95), a post synaptic marker, as well as the AMPA receptor subunits (GluR1 and GluR2/3) and the NMDA receptor NR1. We observed no statistically significant differences in the levels of any of the synaptic proteins in the hippocampus between the 3xTg-saline mice and the WT-saline mice, as determined by Western blots (Fig. 5A,B). However, we found that STZ treatment reduced the levels of synaptophysin and PSD95 in the 3xTg-AD mice. These reductions were confirmed by immunohistochemical studies (Fig. 5C), which also demonstrated the reduction in the cerebral cortex. It is interesting to note that STZ treatment appeared to increase the AMPA receptor subunits in the 3xTg-AD mice, although only the increase of GluR2/3 reached a statistical significance (Fig. 5A,B). Taken together, these results suggest that icv STZ caused deregulation of synaptic proteins and

glutamate receptors in the 3xTg-AD mice, which might disturb synaptic plasticity and underlie the more severe cognitive impairment observed in the 3xTg-STZ mice.

STZ promotes neuroinflammation in 3xTg-AD mice

Neuroinflammation has been implicated in AD, and age-dependent inflammatory response has been reported in the 3xTg-AD mouse brain [31,22,32]. To investigate the effects of STZ treatment on neuroinflammation in the 3xTg-AD mice, we studied glial fibrillary acidic protein (GFAP, an astrocyte marker) and ionized Ca^{2+}-binding adaptor molecule-1 (Iba1, a microglial marker), which are the commonly used markers for glial over-activation and neuroinflammation. In consistent with previous observations, we observed significant increase in both GFAP and Iba1 levels in the hippocampus of the 3xTg-saline mice as compared to the WT-saline mice (Fig. 6A,B), indicating glial over-activation and neuroinflammation. The treatment with STZ further increased the GFAP and Iba1 levels markedly, suggesting STZ's role in promoting neuroinflammation. Immunohistochemical studies indicated that the over-activation of astrocytes and microglia were restricted in the hippocampus of the 3xTg-AD mice (Fig. 6C). However, STZ treatment not only promoted neuroinflammation in the hippocampus, but also induced it throughout the brain in 3xTg-AD mice. Thickened and retracted processes and enlarged soma of both astrocytes and microglia were obvious in the brains of the STZ-treated 3xTg-AD mice (Fig. 6C).

STZ exacerbates dysregulation of brain insulin signaling in 3xTg-AD mice

Brain insulin resistance and insulin deficiency has been observed in AD, and the deficiency worsens with the disease progression [33,10]. We recently observed a dysregulation of brain insulin/insulin-like growth factor-1 (IGF-1) signaling in the brain of both 3xTg-AD mice and icv-STZ mice [34,32]. Therefore, we studied the levels and the activation of each component of the signaling pathway, including insulin receptor (IR), insulin-like growth factor-1 receptor (IGF-1R), insulin receptor substrate-1 (IRS-1), Phosphatidylinositide 3-kinases (PI3K), 3-phosphoinositide-dependent protein kinase-1 (PDK1), Protein Kinase B (AKT) and glycogen synthase kinase-3 (GSK-3). The activation status of these components was assessed by measuring the phosphorylation level of these proteins because their activities are dependent on phosphorylation at specific sites. As observed previously, we found a upregulation of several upstream components (IRS1, IRS1 pS307, PI3K p85 and P-PI3K p85) and a downregulation of several downstream components (PDK1, PKD1 pS241, AKT, AKT pS473, and GSK-3α/β) of the insulin/IGF-1 signaling pathway in the 3xTg-AD mouse brain (Fig. 7A,B). Overall, the STZ treatment exacerbated these alterations.

When the phosphorylation of each component of the insulin/IGF-1 signaling pathway was normalized with the level of the corresponding protein, we found an increase in phosphorylation of AKT and GSK3 in 3xTg-AD mice, which was further enhanced by the STZ treatment (Fig. 7C).

STZ alters expression of AD-related genes in 3xTg-AD mouse brain

We studied the effects of the STZ treatment on gene expression in the 3xTg-AD mouse brains using a customized RT^2 Profiler PCR Array, which included a total of 84 AD-related genes of seven categories (Supplementary Tables S1–S8). Among these 84 genes, we found altered expression of approximately 20 genes in the 3xTg-AD mouse brain previously [34]. Here, we found that the treatment with STZ altered the expression of four genes (*Ide*, *Fos*, *Tsc2*, *Bax*) in the hippocampus (Fig. 8A) and of 13 genes in the cerebral cortex (Fig. 8B) in 3xTg-AD mice. These altered genes included those related to APP processing (*Ide*, *Ctsb*, *Aph1a*, *Mme*), cytoskeleton (*Mapt*, *Nefm*), glucose metabolism and insulin/mTOR signaling (*Tsc2*, *Slc2a4*, *Grb2*, *Pdpk1*), synaptic function (*Ache*, *Chat*), protein kinases (*Mapk8*, *Capn2*), and apoptosis (*Fos*, *Bax*, *Bad*) (Supplementary Tables S2–S8). These results

suggest that icv STZ disturbs multiple metabolic and cell signaling pathways in the 3xTg-AD brain.

Discussion

AD is multifactoral, including various genetic, epigenetic, metabolic, and environmental causes. One common early abnormality in AD is the impairment of brain glucose uptake/metabolism, which occurs many years before the first symptoms appear, raising the possibility that this impairment either is a cause of or is mechanistically involved in AD. In the present study, we treated 6-month-old 3xTg-AD mice (the age before the mice develop typical AD pathologies) with icv STZ and found that the brain administration of STZ exacerbated memory deficits, as well as several AD-related brain abnormalities in the 3xTg-AD mice. Administration of STZ into the brain of WT mice also causes learning and spatial memory deficits, neuroinflammation, altered synaptic proteins and insulin signaling, and hyperphosphorylation of tau in the brain [32]. Taking together, these findings provide experimental evidence demonstrating the role of a brain metabolic insult in AD.

STZ is a diabetogenic compound that is commonly used to produce animal models of diabetes. When administrated intraperitoneally in high doses (45–75 mg/kg), STZ causes the death of insulin producing/secreting pancreatic β cells and induces type 1 diabetes. The pancreatic β cells are most vulnerable to STZ because it enters cells mainly through glucose transporter 2 that is most highly expressed on the plasma membrane of the β cells [35]. Low doses (20–60 mg/kg) of STZ given intraperitoneally in combination of high-fat diets cause insulin resistance and type 2 diabetes [36]. Both type 1 and type 2 diabetic animals produced by peripheral administration of STZ show some aspects of brain abnormalities, including tau hyperphosphorylation, as seen in AD brain [37–39]. Planel et al. demonstrated that the peripheral STZ induces tau hyperphosphorylation through two distinct mechanisms—one is consequent to hypothermia and induced by impaired glucose/energy metabolism, and the other is inherent to insulin deficiency and induced by inhibition of protein phosphatase activities [37]. Increased tau phosphorylation and deregulation of insulin signaling are also seen in the brains of individuals with diabetes [9,10]. The mechanism of central STZ action and its target cells/molecules have not yet been clarified but a similar mechanism of action to that in the periphery might be possible. Glucose transporter 2, which is also expressed in the mammalian brain [40], may also be responsible for the STZ-induced effects in the brain. Our previous [32] and the present studies indicated that STZ causes neuroinflammation, altered synaptic proteins and insulin signaling, and increased hyperphosphorylated tau in the brain.

Progressive memory loss and dementia are the dominant clinical symptoms of AD. The 3xTg-AD mice develop age-dependent memory loss, which starts in 5–6-month old animals [21,41]. As expected, we observed significant impairment of short-term memory and spatial reference memory in the 3xTg-AD mice at the age of 7–8 months, as determined by one-trial object recognition task and Morris water maze test. STZ exacerbated both memory deficits one month post administration of this compound. In addition, the STZ treatment aggravated the anxiety level of the 3xTg-AD mice and caused some loss of body weight. At the age of 7–8 months, the 3xTg-saline mice had zero mortality, and the surgery itself did not cause any death of the animals. However, the 3xTg-STZ mice had approximately 30% mortality. Because the same dose STZ injection did not kill any WT control mice (unpublished observations), icv STZ might have added neurotoxicity onto the 3xTg-AD mice and increased the mortality. Neurotoxicity of central STZ was reported previously [42].

The 3xTg-AD mice develop numerous NFTs after they reach the age of 12 months, but hyperphosphorylation of tau occur at a much earlier age [22,19,32]. The present study demonstrated elevated tau that was phosphorylated at multiple AD-related phosphorylation sites in the 3xTg-AD mice at the age of 7–8 months. The icv STZ administration further increased the accumulation of tau that was phosphorylated at several of these sites. These results suggest that the central STZ exacerbates tau pathology in the 3xTg-AD mice. These findings are consistent with previous reports showing an increase in tau phosphorylation after icv administration of STZ in rodents [12,13,32].

Deposition of Aβ peptides into amyloid plaques is one of the hallmark pathologies of AD, but whether Aβ accumulation is a cause of neurodegeneration and memory loss is still under debate. Although icv STZ administration exacerbated both short-term memory and spatial reference memory, we found that it lowered, rather than increased, both $A\beta_{1–42}$ and $A\beta_{1–40}$ in the brain of the 3xTg-AD mice. These results indicate that the STZ-induced worsening of cognitive function observed in the present study is unrelated to brain Aβ level. The STZ-induced reduction of Aβ might result from reduced processing from APP into Aβ or increased Aβ turnover, or both, because the APP level was not altered by icv STZ administration. We recently found that icv STZ administration reduces the expression of presenilin 1, the catalytic subunit of γ-secretase, in the mouse hippocampus [34]. Thus, icv STZ might have led to reduced Aβ production in the mouse brain. Because STZ induces marked glial activation in the brain [43,44,32], it is also likely that the activated astrocytes and microglia had helped the clearance of Aβ in the 3xTg-AD brain. It is well known that these glial cells help the clearance of Aβ [45–47]. It should be noted that the Tg2576 mice, which over-express mutated APP in the brain, show increased aggregation and level of Aβ as well as exacerbation of memory deficits 6 months after icv administration of STZ [48]. It appears that icv STZ administration may first decrease (as we observed 6 weeks after STZ injection) and then increase Aβ level. Future studies of the expression and processing of APP and the degradation of Aβ of the mouse brains at various periods of time after icv STZ administration may reveal the mechanism of this possible dynamic change of Aβ.

We also noticed that the human $A\beta_{1–42}/A\beta_{1–40}$ ratio was approximately 1.5 in the 3xTg-AD brain, which is consistent with previous studies showing higher level of $A\beta_{1–42}$ than $A\beta_{1–40}$ in the 3xTg-AD mouse brains at the age of 6–9 months old [49]. Much higher levels of $A\beta_{1–42}$ than $A\beta_{1–40}$ are also seen in the brains of AD patients [50].

Synaptic dysfunction and loss are known to occur at early stage of AD and correlate with cognitive severity better than amyloid plaques and NFTs [51–54]. At 6 months of age, deficits in long-term potentiation are already apparent in the 3xTg-AD mice [18], although synaptic loss, as evidenced by levels of synaptophysin and PSD95, was not obvious. We observed that the icv STZ treatment reduced the levels of both synaptophysin and PSD95 in the hippocampus of the 3xTg-AD mice, suggesting a substantial loss of synapses caused by STZ. The effects of STZ on synapses might underlie its activity to exacerbate the memory deficits of the 3xTg-AD mice. The STZ-induced reduction of synaptophysin and PSD95 was unlikely due to decreased expression, because no reduction of the mRNA levels was observed by quantitative PCR array. We also investigated the levels of AMPA receptor subunits (GluR1 and GluR2/3) and the NMDA receptor NR1, which mediate synaptic transmission and plasticity [55,56]. Unlike a recent study showing that STZ decreased the level of GluR1 in the rat hippocampus [57], we did not observe such a reduction.

Neuroinflammation, as reflected by activation of microglia and astrocytes, is believed to be involved in the pathogenesis of AD [58]. Epidemiological studies have demonstrated that anti-inflammatory drug use reduces the risk or delay the onset of AD [58]. Although the exact trigger of neuroinflammation in AD brain remains elusive, its interactions with Aβ and

tau, as seen in both AD brain and animal models, may promote the progression of the AD pathology [59,46]. In consistent with a previous study [22], we also observed activation of both microglia and astrocytes in the hippocampus of 3xTg-AD mice. After icv administration of STZ, a very marked increase in microglia and astrocytes was observed not only in the hippocampus, but also in the cerebral cortex, cerebellum and brain stem. These results are consistent with marked glial activation in the brain of non-Tg rodent model produced by icv STZ administration [43,44,32]. The lack of region specificity of STZ-induced neuroinflammation was mainly because STZ reached the whole brain with the circulation of CSF after icv injection. This might also explain the impaired performance of the 3xTg-STZ mice on the Rotarod and the reduced swim speed in Morris water maze, which might have resulted from STZ-induced compromised cerebellum function.

Decreased brain glucose/energy metabolism has been established in AD decades ago. We recently found disturbed brain insulin signaling in AD [10], which may partially explain the decreased brain glucose/energy metabolism. In the present study, we found that brain insulin signaling was also disturbed in the brains of 3xTg-AD mice. The icv administration of STZ further exacerbated the dysregulation of insulin signaling in the mouse brain. Intranasal insulin treatment was reported to improve cerebral glucose metabolism and cognition both in rodents and in AD and mildly cognitively impaired adults [60–64]. STZ's exacerbation of the disturbance of brain insulin signaling could therefore be responsible for the worsened cognitive impairment we observed in the 3xTg-STZ mice. It is worth to note that in the brains of 3xTg-AD mice, several upstream components (IRS1, IRS1 pS307, PI3K p85 and P-PI3K p85) of the insulin signaling pathway were found to be upregulated, whereas several downstream components (PDK1, PKD1 pS241, AKT, AKT pS473, and GSK3α/β) downregulated. The upregulation of the upstream components may result from a compensatory response to the STZ-induced downregulation of the downstream signaling and is consistent to a previous study showing elevated tyrosine kinase activity of IR in the icv-STZ rat brains [13].

Epidemiological studies have demonstrated that diabetes is a risk factor for AD [65,66]. Periphery administration of STZ to induce peripheral insulin deficiency (i.e., type 1 diabetes) disturbs brain insulin signaling and promotes Aβ production, neuritic plaque formation and spatial memory deficits in transgenic AD mouse models [67,68]. AD-like brain abnormalities are also seen in rodents with experimental insulin resistance and type 2 diabetes [69,39]. Therefore, it appears that the peripheral metabolic insults may also affect the metabolism in the brain and promote neurodegeneration.

In conclusion, we demonstrated that the central administration of STZ exacerbated impairment of short-term memory and spatial reference memory in 3xTg-AD mice. The STZ treatment also resulted in an increase of tau hyperphosphorylation and neuroinflammation, a disturbance of brain insulin signaling, a decrease of synaptic plasticity and amyloid β peptides, and altered expression of 20 AD-related genes in the brains of 3xTg-AD mice. These findings demonstrate the role of metabolic insult in AD pathology in vivo.

Supplementary Material

Refer to Web version on PubMed Central for supplementary material.

Acknowledgments

We thank F.M. LaFerla of University of California, Irvine, for providing the breeding pairs of 3xTg-AD mouse, and Ms. J. Murphy for secretarial assistance. This work was supported in part by the New York State Office for People with Developmental Disabilities as well as grants from the National Institutes of Health (R01 AG027429, R03

TW008123), the U.S. Alzheimer's Association (IIRG-10-170405 and IIRG-10-173154), the National Key Basic Research Program of China (2013CB530900), and the Wuhan Science and Technology Bureau, China (200960323132). The funders had no role in study design, data collection and analysis, decision to publish, or preparation of the manuscript.

References

1. Iqbal K, Wang X, Blanchard J, Liu F, Gong CX, Grundke-Iqbal I. Alzheimer's disease neurofibrillary degeneration: pivotal and multifactorial. Biochem Soc Trans. 2010; 38(4):962–966. [PubMed: 20658985]
2. Casadesus G, Moreira PI, Nunomura A, Siedlak SL, Bligh-Glover W, Balraj E, Petot G, Smith MA, Perry G. Indices of metabolic dysfunction and oxidative stress. Neurochem Res. 2007; 32(4–5): 717–722. [PubMed: 17342408]
3. de Leon MJ, Ferris SH, George AE, Reisberg B, Christman DR, Kricheff II, Wolf AP. Computed tomography and positron emission transaxial tomography evaluations of normal aging and Alzheimer's disease. J Cereb Blood Flow Metab. 1983; 3(3):391–394. [PubMed: 6603463]
4. Hoyer S. Glucose metabolism and insulin receptor signal transduction in Alzheimer disease. Eur J Pharmacol. 2004; 490(1–l3):115–125. [PubMed: 15094078]
5. Reiman EM, Caselli RJ, Chen K, Alexander GE, Bandy D, Frost J. Declining brain activity in cognitively normal apolipoprotein E epsilon 4 heterozygotes: A foundation for using positron emission tomography to efficiently test treatments to prevent Alzheimer's disease. Proc Natl Acad Sci U S A. 2001; 98(6):3334–3339. [PubMed: 11248079]
6. Smith GS, de Leon MJ, George AE, Kluger A, Volkow ND, McRae T, Golomb J, Ferris SH, Reisberg B, Ciaravino J, et al. Topography of cross-sectional and longitudinal glucose metabolic deficits in Alzheimer's disease. Pathophysiologic implications. Arch Neurol. 1992; 49(11):1142–1150. [PubMed: 1444881]
7. Heiss WD, Szelies B, Kessler J, Herholz K. Abnormalities of energy metabolism in Alzheimer's disease studied with PET. Ann N Y Acad Sci. 1991; 640:65–71. [PubMed: 1776760]
8. Mosconi L. Brain glucose metabolism in the early and specific diagnosis of Alzheimer's disease. FDG-PET studies in MCI and AD. Eur J Nucl Med Mol Imaging. 2005; 32(4):486–510. [PubMed: 15747152]
9. Liu Y, Liu F, Grundke-Iqbal I, Iqbal K, Gong CX. Brain glucose transporters, OGlcNAcylation and phosphorylation of tau in diabetes and Alzheimer's disease. J Neurochem. 2009; 111(1):242–249. [PubMed: 19659459]
10. Liu Y, Liu F, Grundke-Iqbal I, Iqbal K, Gong CX. Deficient brain insulin signalling pathway in Alzheimer's disease and diabetes. J Pathol. 2011; 225(1):54–62. [PubMed: 21598254]
11. Liu Y, Liu F, Iqbal K, Grundke-Iqbal I, Gong CX. Decreased glucose transporters correlate to abnormal hyperphosphorylation of tau in Alzheimer disease. FEBS Lett. 2008; 582(2):359–364. [PubMed: 18174027]
12. Deng Y, Li B, Liu Y, Iqbal K, Grundke-Iqbal I, Gong CX. Dysregulation of insulin signaling, glucose transporters, O-GlcNAcylation, and phosphorylation of tau and neurofilaments in the brain: Implication for Alzheimer's disease. Am J Pathol. 2009; 175(5):2089–2098. [PubMed: 19815707]
13. Grunblatt E, Salkovic-Petrisic M, Osmanovic J, Riederer P, Hoyer S. Brain insulin system dysfunction in streptozotocin intracerebroventricularly treated rats generates hyperphosphorylated tau protein. J Neurochem. 2007; 101(3):757–770. [PubMed: 17448147]
14. Salkovic-Petrisic M, Hoyer S. Central insulin resistance as a trigger for sporadic Alzheimer-like pathology: an experimental approach. J Neural Transm Suppl. 2007; (72):217–233. [PubMed: 17982898]
15. Hoyer S, Lannert H. Long-term abnormalities in brain glucose/energy metabolism after inhibition of the neuronal insulin receptor: implication of tau-protein. J Neural Transm Suppl. 2007; (72): 195–202. [PubMed: 17982895]
16. Nitsch R, Hoyer S. Local action of the diabetogenic drug, streptozotocin, on glucose and energy metabolism in rat brain cortex. Neurosci Lett. 1991; 128(2):199–202. [PubMed: 1834965]

17. Janelsins MC, Mastrangelo MA, Oddo S, LaFerla FM, Federoff HJ, Bowers WJ. Early correlation of microglial activation with enhanced tumor necrosis factor-alpha and monocyte chemoattractant protein- expression specifically within the entorhinal cortex of triple transgenic Alzheimer's disease mice. J Neuroinflammation. 2005; 2:23. [PubMed: 16232318]
18. Oddo S, Caccamo A, Shepherd JD, Murphy MP, Golde TE, Kayed R, Metherate R, Mattson MP, Akbari Y, LaFerla FM. Triple-transgenic model of Alzheimer's disease with plaques and tangles: intracellular Abeta and synaptic dysfunction. Neuron. 2003; 39(3):409–421. [PubMed: 12895417]
19. Oddo S, Caccamo A, Kitazawa M, Tseng BP, LaFerla FM. Amyloid deposition precedes tangle formation in a triple transgenic model of Alzheimer's disease. Neurobiol Aging. 2003; 24(8): 1063–1070. [PubMed: 14643377]
20. Billings LM, Oddo S, Green KN, McGaugh JL, LaFerla FM. Intraneuronal Abeta causes the onset of early Alzheimer's disease-related cognitive deficits in transgenic mice. Neuron. 2005; 45(5): 675–688. [PubMed: 15748844]
21. Clinton LK, Billings LM, Green KN, Caccamo A, Ngo J, Oddo S, McGaugh JL, LaFerla FM. Age-dependent sexual dimorphism in cognition and stress response in the 3xTg-AD mice. Neurobiol Dis. 2007; 28(1):76–82. [PubMed: 17659878]
22. Mastrangelo MA, Bowers WJ. Detailed immunohistochemical characterization of temporal and spatial progression of Alzheimer's disease-related pathologies in male triple-transgenic mice. BMC Neurosci. 2008; 9:81. [PubMed: 18700006]
23. Sargolini F, Roullet P, Oliverio A, Mele A. Effects of intra-accumbens focal administrations of glutamate antagonists on object recognition memory in mice. Behav Brain Res. 2003; 138(2):153–163. [PubMed: 12527446]
24. Morris RG, Garrud P, Rawlins JN, O'Keefe J. Place navigation impaired in rats with hippocampal lesions. Nature. 1982; 297(5868):681–683. [PubMed: 7088155]
25. Bensadoun A, Weinstein D. Assay of proteins in the presence of interfering materials. Anal Biochem. 1976; 70(1):241–250. [PubMed: 1259145]
26. Blanchard J, Wanka L, Tung YC, Cardenas-Aguayo Mdel C, LaFerla FM, Iqbal K, Grundke-Iqbal I. Pharmacologic reversal of neurogenic and neuroplastic abnormalities and cognitive impairments without affecting Abeta and tau pathologies in 3xTg-AD mice. Acta Neuropathol. 2010; 120(5): 605–621. [PubMed: 20697724]
27. Pellow S, Chopin P, File SE, Briley M. Validation of open:closed arm entries in an elevated plus-maze as a measure of anxiety in the rat. J Neurosci Methods. 1985; 14(3):149–167. [PubMed: 2864480]
28. Clark RE, Zola SM, Squire LR. Impaired recognition memory in rats after damage to the hippocampus. J Neurosci. 2000; 20(23):8853–8860. [PubMed: 11102494]
29. Ennaceur A, Aggleton JP. The effects of neurotoxic lesions of the perirhinal cortex combined to fornix transection on object recognition memory in the rat. Behav Brain Res. 1997; 88(2):181–193. [PubMed: 9404627]
30. Ennaceur A, Neave N, Aggleton JP. Spontaneous object recognition and object location memory in rats: the effects of lesions in the cingulate cortices, the medial prefrontal cortex, the cingulum bundle and the fornix. Exp Brain Res. 1997; 113(3):509–519. [PubMed: 9108217]
31. Kitazawa M, Oddo S, Yamasaki TR, Green KN, LaFerla FM. Lipopolysaccharideinduced inflammation exacerbates tau pathology by a cyclin-dependent kinase 5-mediated pathway in a transgenic model of Alzheimer's disease. J Neurosci. 2005; 25(39):8843–8853. [PubMed: 16192374]
32. Chen Y, Liang Z, Blanchard J, Dai CL, Sun S, Lee MH, Grundke-Iqbal I, Iqbal K, Liu F, Gong CX. A non-transgenic mouse model (icv-STZ mouse) of Alzheimer's disease: similarities to and differences from the transgenic model (3xTg-AD mouse). Mol Neurobiol. 2013; 47(2):711–725. [PubMed: 23150171]
33. de la Monte SM. Brain insulin resistance and deficiency as therapeutic targets in Alzheimer's disease. Curr Alzheimer Res. 2012; 9(1):35–66. [PubMed: 22329651]
34. Chen Y, Tian Z, Liang Z, Sun S, Dai CL, Lee MH, Laferla FM, Grundke-Iqbal I, Iqbal K, Liu F, Gong CX. Brain Gene Expression of a Sporadic (icv-STZ Mouse) and a Familial Mouse Model (3xTg-AD Mouse) of Alzheimer's Disease. PLoS One. 2012; 7(12):e51432. [PubMed: 23236499]

35. Szkudelski T. The mechanism of alloxan and streptozotocin action in B cells of the rat pancreas. Physiol Res. 2001; 50(6):537–546. [PubMed: 11829314]
36. Blondel O, Portha B. Early appearance of in vivo insulin resistance in adult streptozotocin-injected rats. Diabete Metab. 1989; 15(6):382–387. [PubMed: 2697607]
37. Planel E, Tatebayashi Y, Miyasaka T, Liu L, Wang L, Herman M, Yu WH, Luchsinger JA, Wadzinski B, Duff KE, Takashima A. Insulin dysfunction induces in vivo tau hyperphosphorylation through distinct mechanisms. J Neurosci. 2007; 27(50):13635–13648. [PubMed: 18077675]
38. Jolivalt CG, Hurford R, Lee CA, Dumaop W, Rockenstein E, Masliah E. Type 1 diabetes exaggerates features of Alzheimer's disease in APP transgenic mice. Exp Neurol. 2010; 223(2): 422–431. [PubMed: 19931251]
39. Yang Y, Ma D, Wang Y, Jiang T, Hu S, Zhang M, Yu X, Gong CX. Intranasal insulin ameliorates tau hyperphosphorylation in a rat model of type 2 diabetes. J Alzheimers Dis. 2013; 33(2):329–338. [PubMed: 22936005]
40. Arluison M, Quignon M, Nguyen P, Thorens B, Leloup C, Penicaud L. Distribution and anatomical localization of the glucose transporter 2 (GLUT2) in the adult rat brain--an immunohistochemical study. J Chem Neuroanat. 2004; 28(3):117–136. [PubMed: 15482899]
41. Gimenez-Llort L, Blazquez G, Canete T, Johansson B, Oddo S, Tobena A, LaFerla FM, Fernandez-Teruel A. Modeling behavioral and neuronal symptoms of Alzheimer's disease in mice: a role for intraneuronal amyloid. Neurosci Biobehav Rev. 2007; 31(1):125–147. [PubMed: 17055579]
42. Mayer G, Nitsch R, Hoyer S. Effects of changes in peripheral and cerebral glucose metabolism on locomotor activity, learning and memory in adult male rats. Brain Res. 1990; 532(1–2):95–100. [PubMed: 2149302]
43. Prickaerts J, Fahrig T, Blokland A. Cognitive performance and biochemical markers in septum, hippocampus and striatum of rats after an i.c.v. injection of streptozotocin: a correlation analysis. Behav Brain Res. 1999; 102(1–2):73–88. [PubMed: 10403017]
44. Rodrigues L, Biasibetti R, Swarowsky A, Leite MC, Quincozes-Santos A, Quilfeldt JA, Achaval M, Goncalves CA. Hippocampal alterations in rats submitted to streptozotocin-induced dementia model are prevented by aminoguanidine. J Alzheimers Dis. 2009; 17(1):193–202. [PubMed: 19494442]
45. Heneka MT, O'Banion MK. Inflammatory processes in Alzheimer's disease. J Neuroimmunol. 2007; 184(1–2):69–91. [PubMed: 17222916]
46. Weitz TM, Town T. Microglia in Alzheimer's Disease: It's All About Context. Int J Alzheimers Dis. 2012; 2012:314185. [PubMed: 22779026]
47. Wyss-Coray T, Loike JD, Brionne TC, Lu E, Anankov R, Yan F, Silverstein SC, Husemann J. Adult mouse astrocytes degrade amyloid-beta in vitro and in situ. Nat Med. 2003; 9(4):453–457. [PubMed: 12612547]
48. Plaschke K, Kopitz J, Siegelin M, Schliebs R, Salkovic-Petrisic M, Riederer P, Hoyer S. Insulin-resistant brain state after intracerebroventricular streptozotocin injection exacerbates Alzheimer-like changes in Tg2576 AbetaPP-overexpressing mice. J Alzheimers Dis. 2010; 19(2):691–704. [PubMed: 20110613]
49. Martinez-Coria H, Green KN, Billings LM, Kitazawa M, Albrecht M, Rammes G, Parsons CG, Gupta S, Banerjee P, LaFerla FM. Memantine improves cognition and reduces Alzheimer's-like neuropathology in transgenic mice. Am J Pathol. 2010; 176(2):870–880. [PubMed: 20042680]
50. Wang J, Dickson DW, Trojanowski JQ, Lee VM. The levels of soluble versus insoluble brain Abeta distinguish Alzheimer's disease from normal and pathologic aging. Exp Neurol. 1999; 158(2):328–337. [PubMed: 10415140]
51. Arendt T. Synaptic degeneration in Alzheimer's disease. Acta Neuropathol. 2009; 118(1):167–179. [PubMed: 19390859]
52. DeKosky ST, Scheff SW. Synapse loss in frontal cortex biopsies in Alzheimer's disease: correlation with cognitive severity. Ann Neurol. 1990; 27(5):457–464. [PubMed: 2360787]
53. Selkoe DJ. Alzheimer's disease is a synaptic failure. Science. 2002; 298(5594):789–791. [PubMed: 12399581]

54. Terry RD, Masliah E, Salmon DP, Butters N, DeTeresa R, Hill R, Hansen LA, Katzman R. Physical basis of cognitive alterations in Alzheimer's disease: synapse loss is the major correlate of cognitive impairment. Ann Neurol. 1991; 30(4):572–580. [PubMed: 1789684]
55. Kloda A, Martinac B, Adams DJ. Polymodal regulation of NMDA receptor channels. Channels (Austin). 2007; 1(5):334–343. [PubMed: 18690040]
56. Malinow R, Malenka RC. AMPA receptor trafficking and synaptic plasticity. Annu Rev Neurosci. 2002; 25:103–126. [PubMed: 12052905]
57. Shonesy BC, Thiruchelvam K, Parameshwaran K, Rahman EA, Karuppagounder SS, Huggins KW, Pinkert CA, Amin R, Dhanasekaran M, Suppiramaniam V. Central insulin resistance and synaptic dysfunction in intracerebroventricular-streptozotocin injected rodents. Neurobiol Aging. 2012; 33(2):430 e435–418. [PubMed: 21256630]
58. Wyss-Coray T, Rogers J. Inflammation in Alzheimer disease-a brief review of the basic science and clinical literature. Cold Spring Harb Perspect Med. 2012; 2(1):a006346. [PubMed: 22315714]
59. Arnaud L, Robakis NK, Figueiredo-Pereira ME. It may take inflammation, phosphorylation and ubiquitination to 'tangle' in Alzheimer's disease. Neurodegener Dis. 2006; 3(6):313–319. [PubMed: 16954650]
60. Craft S, Baker LD, Montine TJ, Minoshima S, Watson GS, Claxton A, Arbuckle M, Callaghan M, Tsai E, Plymate SR, Green PS, Leverenz J, Cross D, Gerton B. Intranasal insulin therapy for Alzheimer disease and amnestic mild cognitive impairment: a pilot clinical trial. Arch Neurol. 2012; 69(1):29–38. [PubMed: 21911655]
61. Francis G, Martinez J, Liu W, Nguyen T, Ayer A, Fine J, Zochodne D, Hanson LR, Frey WH 2nd, Toth C. Intranasal insulin ameliorates experimental diabetic neuropathy. Diabetes. 2009; 58(4): 934–945. [PubMed: 19136650]
62. Francis GJ, Martinez JA, Liu WQ, Xu K, Ayer A, Fine J, Tuor UI, Glazner G, Hanson LR, Frey WH 2nd, Toth C. Intranasal insulin prevents cognitive decline, cerebral atrophy and white matter changes in murine type I diabetic encephalopathy. Brain. 2008; 131(Pt 12):3311–3334. [PubMed: 19015157]
63. Marks DR, Tucker K, Cavallin MA, Mast TG, Fadool DA. Awake intranasal insulin delivery modifies protein complexes and alters memory, anxiety, and olfactory behaviors. J Neurosci. 2009; 29(20):6734–6751. [PubMed: 19458242]
64. Reger MA, Watson GS, Green PS, Baker LD, Cholerton B, Fishel MA, Plymate SR, Cherrier MM, Schellenberg GD, Frey WH 2nd, Craft S. Intranasal insulin administration dose-dependently modulates verbal memory and plasma amyloid-beta in memory-impaired older adults. J Alzheimers Dis. 2008; 13(3):323–331. [PubMed: 18430999]
65. Kopf D, Frolich L. Risk of incident Alzheimer's disease in diabetic patients: a systematic review of prospective trials. J Alzheimers Dis. 2009; 16(4):677–685. [PubMed: 19387104]
66. Sims-Robinson C, Kim B, Rosko A, Feldman EL. How does diabetes accelerate Alzheimer disease pathology? Nature reviews. 2010; 6(10):551–559.
67. Wang X, Zheng W, Xie JW, Wang T, Wang SL, Teng WP, Wang ZY. Insulin deficiency exacerbates cerebral amyloidosis and behavioral deficits in an Alzheimer transgenic mouse model. Mol Neurodegener. 2010; 5:46. [PubMed: 21044348]
68. Devi L, Alldred MJ, Ginsberg SD, Ohno M. Mechanisms underlying insulin deficiency-induced acceleration of beta-amyloidosis in a mouse model of Alzheimer's disease. PLoS One. 2012; 7(3):e32792. [PubMed: 22403710]
69. Ho L, Qin W, Pompl PN, Xiang Z, Wang J, Zhao Z, Peng Y, Cambareri G, Rocher A, Mobbs CV, Hof PR, Pasinetti GM. Diet-induced insulin resistance promotes amyloidosis in a transgenic mouse model of Alzheimer's disease. FASEB J. 2004; 18(7):902–904. [PubMed: 15033922]
70. Tatebayashi Y, Iqbal K, Grundke-Iqbal I. Dynamic regulation of expression and phosphorylation of tau by fibroblast growth factor-2 in neural progenitor cells from adult rat hippocampus. J Neurosci. 1999; 19(13):5245–5254. [PubMed: 10377336]
71. Pei JJ, Gong CX, Iqbal K, Grundke-Iqbal I, Wu QL, Winblad B, Cowburn RF. Subcellular distribution of protein phosphatases and abnormally phosphorylated tau in the temporal cortex from Alzheimer's disease and control brains. J Neural Transm. 1998; 105(1):69–83. [PubMed: 9588762]

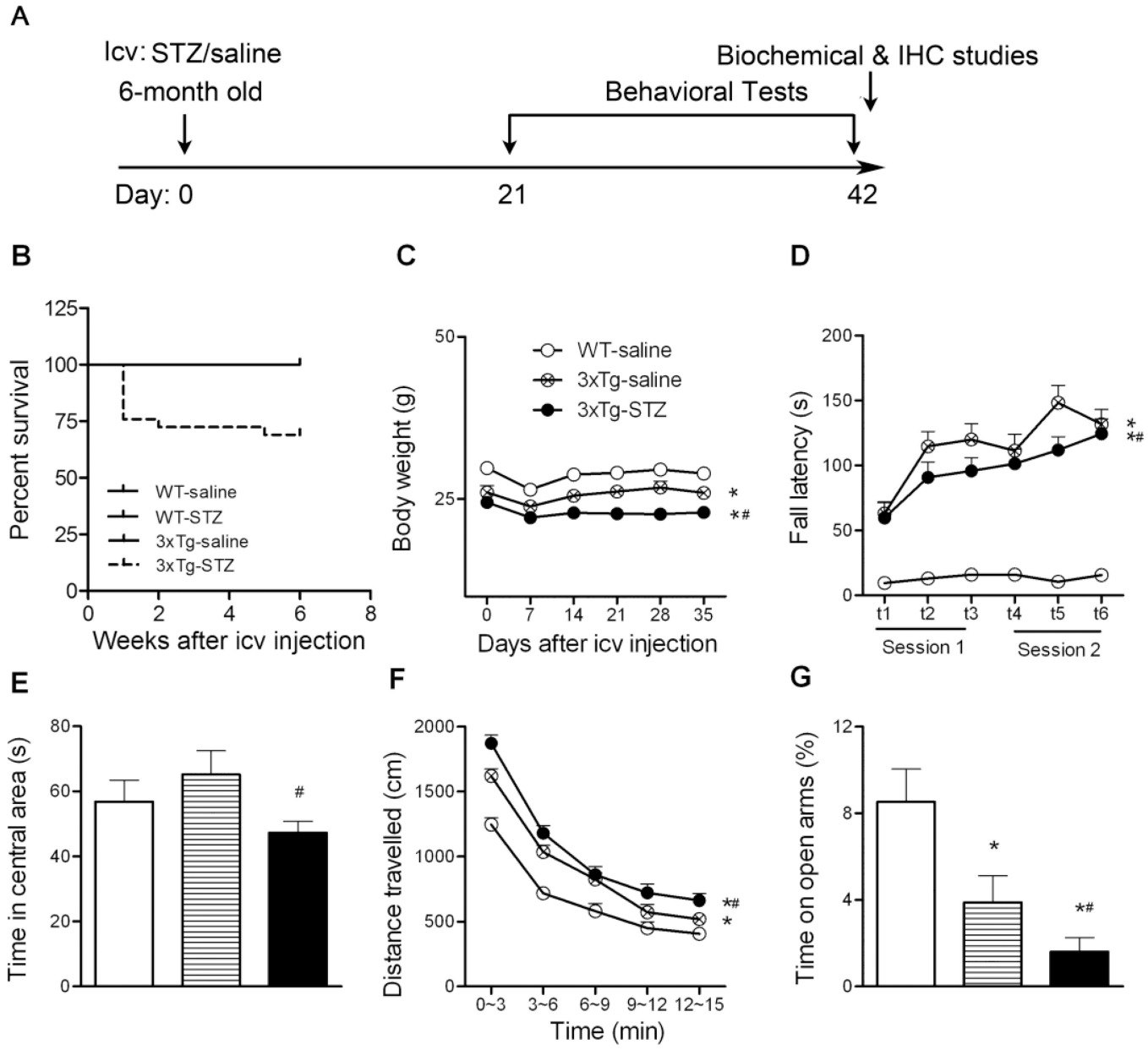

Fig. 1.

Animal experimental schematics (A) and general behavior characterization (B-G). B, Survival rate 42 days after icv STZ injection. C, The body weights of the mice after icv injection were monitored once a week. D, Motor coordination and balance were evaluated using accelerating Rotarod. E-F, Spontaneous locomotor and exploratory activity was assessed in an open field, and the time spent in the central area (E) and the total distance traveled in the open field (F) are shown. G, Anxiety-like behavior was assessed in the elevated plus maze by measuring the percentage of time spent on open arms. $^{*}p < 0.05$ vs. WT-saline; $^{\#}p < 0.05$ vs. 3xTg-saline.

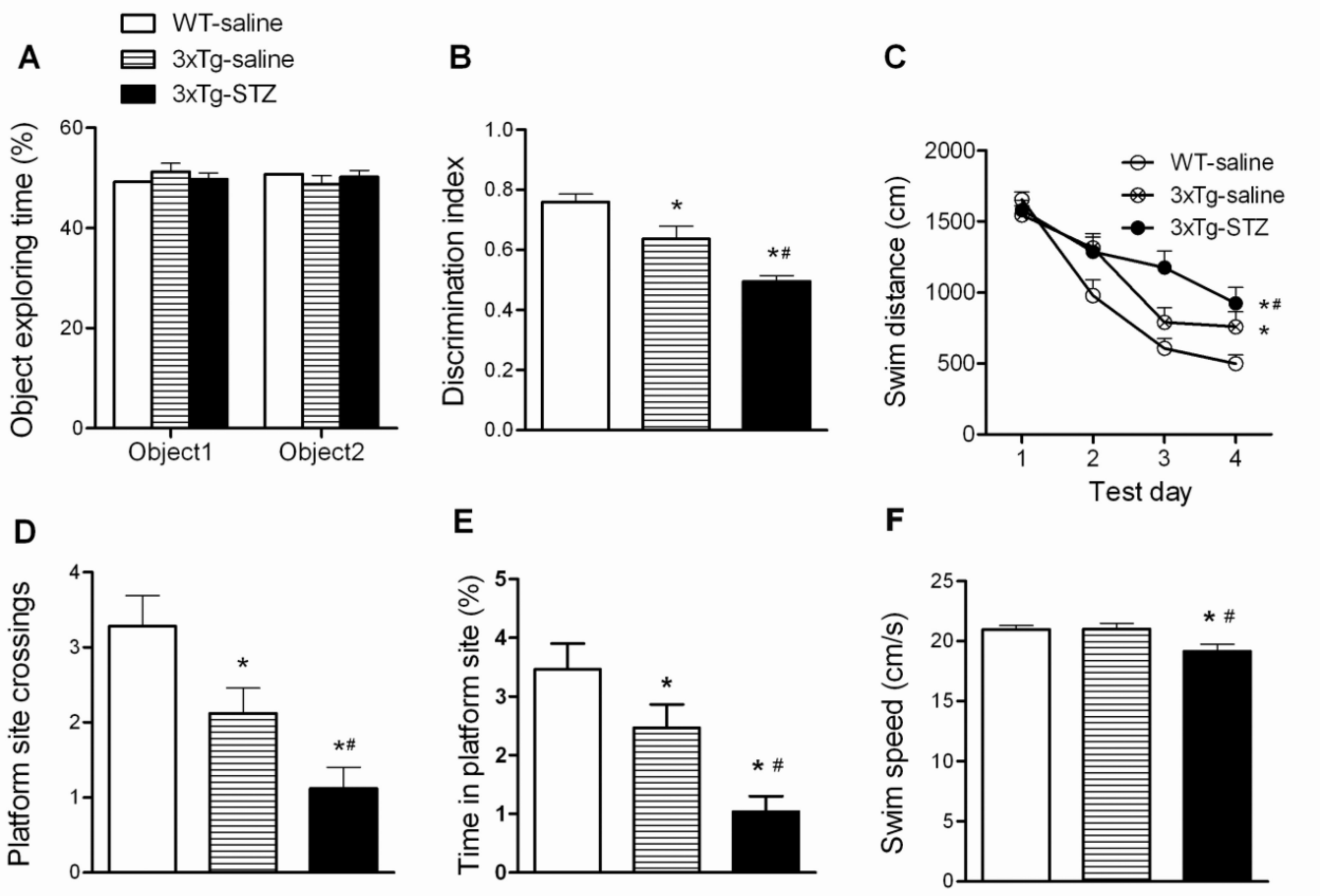

Fig. 2.

Behavioral tests of mice using one-trial object recognition task and Morris water maze. One-trial object recognition task was carried out in an open field arena. Time spent exploring two identical objects during the sample phase are shown as percentage of object exploring time (A). Object discrimination during the test phase is presented by a discrimination index (time exploring the novel object / total time for exploring) (B). Spatial reference learning and memory were tested in Morris water maze (C-F). Distance traveled to the hidden platform in the water maze during training (C), number of platform site crossings (D) and percentage of time spent at the platform site (E) during the probe trial, and the average swim speed during the water maze task (F) are shown. $^{*}p < 0.05$ vs. WT-saline. $^{\#}p < 0.05$ 3xTg-STZ vs. 3xTg-saline.

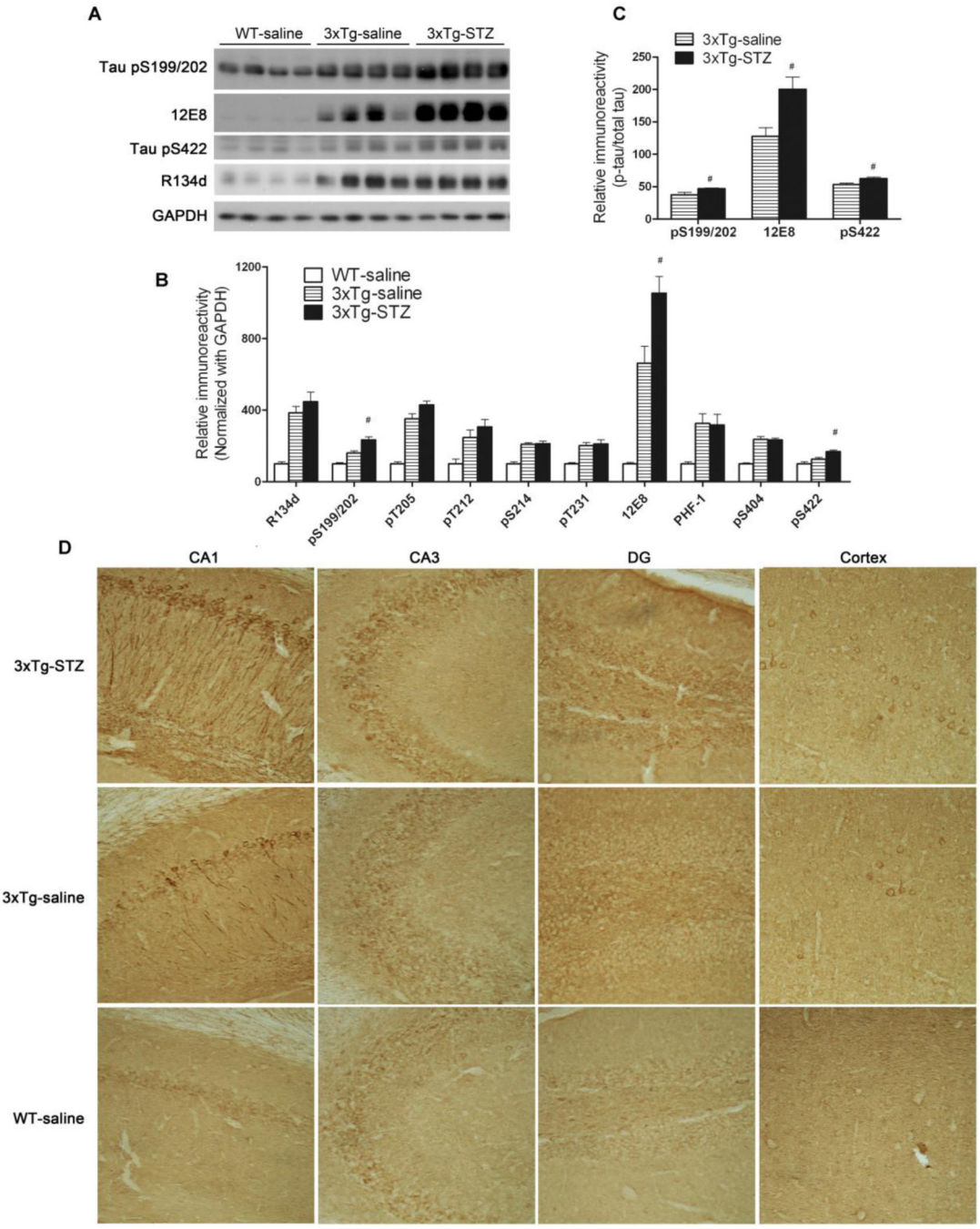

Fig. 3.

Effect of icv STZ treatment on tau phosphorylation in 3xTg-AD mice. (A) Homogenates of the hippocampi from WT-saline, 3xTg-saline and 3xTg-STZ mice were analyzed by Western blots developed with antibody R134d against total tau and with several phosphorylation-dependent and site-specific tau antibodies. (B, C) Densitometrical quantification of the blots after normalization with the GAPDH level (B) or with the total tau level (C). $^{\#}p < 0.05$ 3xTg-STZ vs. 3xTg-saline. (D) Immunohistochemical staining of mouse brain sections with pS199/202 against tau phosphorylated at these sites. Representative staining of the CA1 and CA3 sectors of the hippocampus, dentate gyrus (DG), and the cerebral cortex is shown (magnification: 20x).

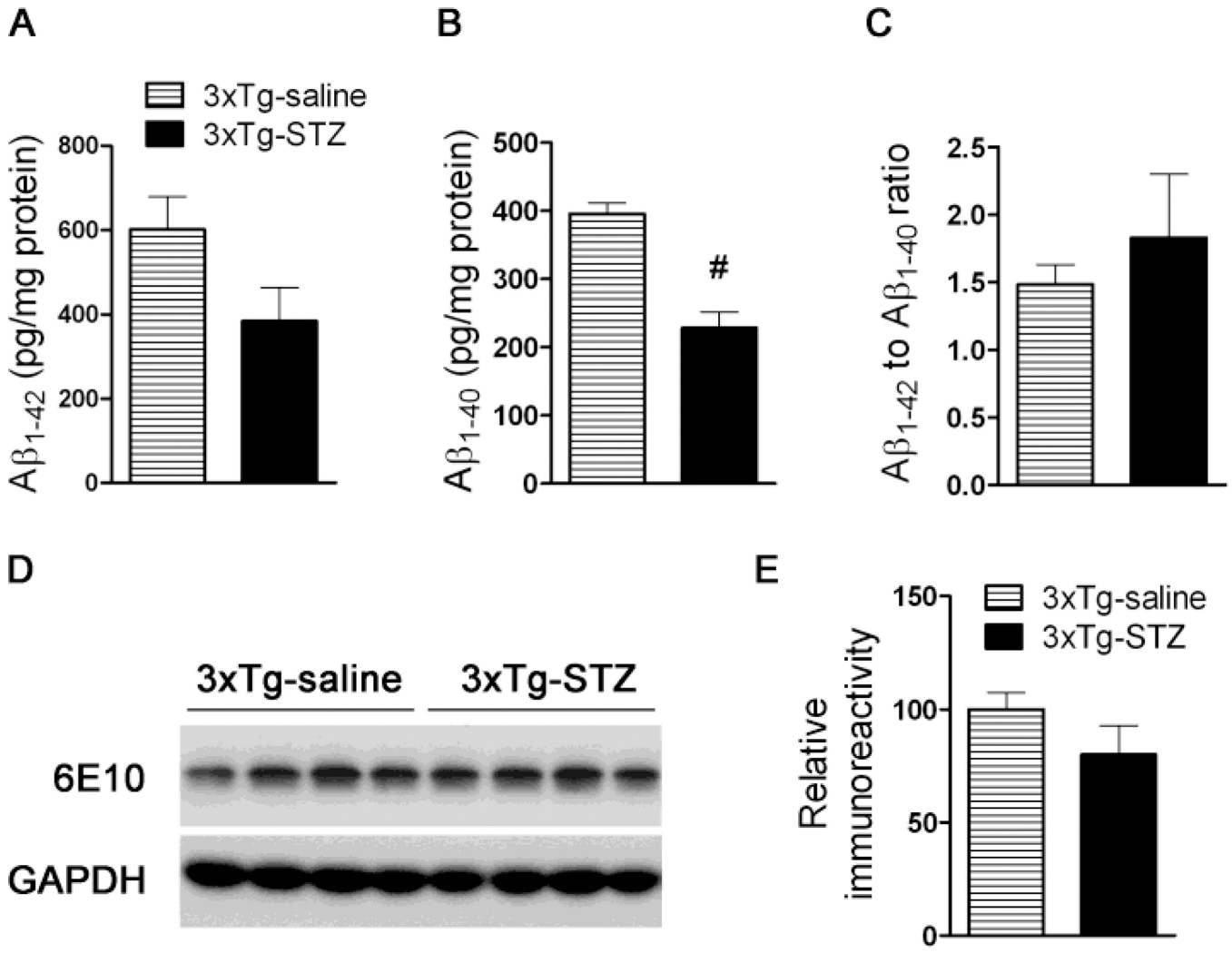

Fig. 4.

Effect of icv STZ on the levels of $A\beta_{1–42}A\beta_{1–40}$ and APP in 3xTg-AD mice. (A-C) The levels of human $A\beta_{1–42}$ (A) and $A\beta_{1–40}$ (B) in the mouse hippocampal tissue were measured by ELISA, and the $A\beta_{1–42}/A\beta_{1–40}$ ratio was calculated (C). $^{\#}p < 0.05$ vs. 3xTg-saline group (n=10/group). (D) Western blots of the hippocampal homogenates developed with antibody 6E10 against human APP. (E) Quantification of APP blots (n=10) after normalization with GAPDH.

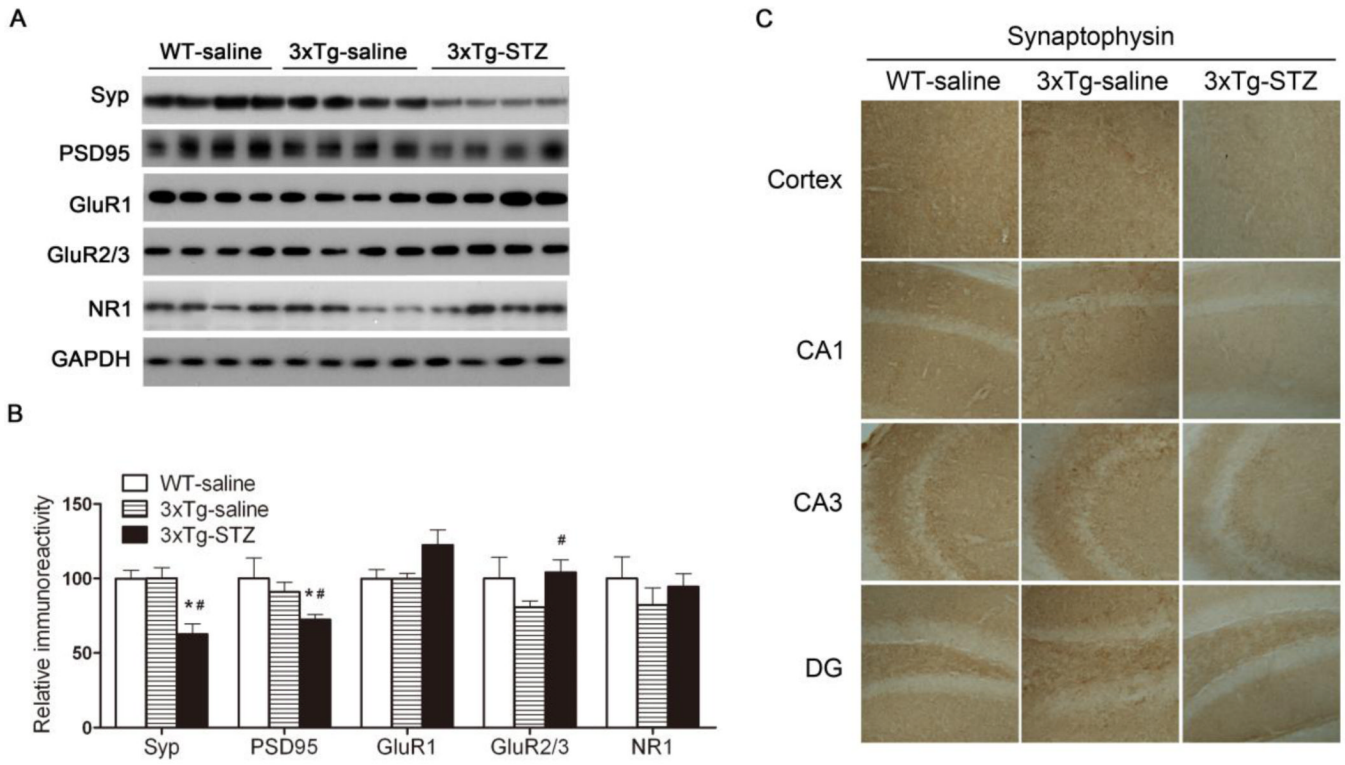

Fig. 5.

Synaptic proteins in WT-saline, 3xTg-saline and 3xTg-STZ mice. (A) Hippocampal homogenates were analyzed by Western blots developed with antibodies indicated on the left of the blots. (B) Densitometrical quantification of the blots after normalization with GAPDH level. $^{*}p < 0.05$ vs. WT-saline; $^{\#}p < 0.05$ vs. 3xTg-saline. (C) Representative immunohistochemical staining of the frozen tissue sections of the mouse brains (magnification: 20x).

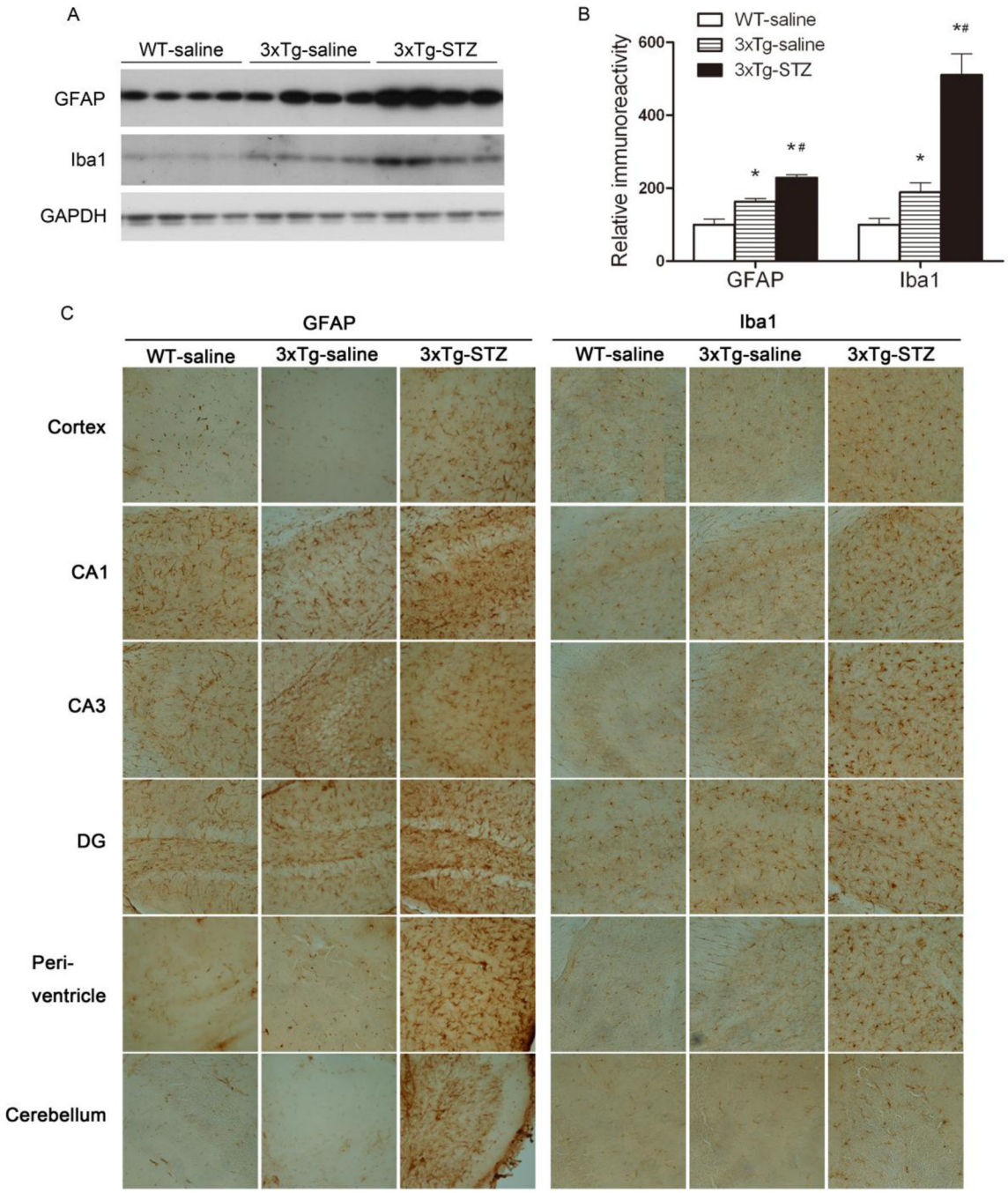

Fig. 6.

Promotion of neuroinflammation by icv STZ in 3xTg-AD mice. (A) Homogenates of the hippocampi from WT-saline, 3xTg-saline and 3xTg-STZ mice were analyzed by Western blots developed with antibodies against GFAP and Iba1, and, as a loading control, GAPDH. (B) Densitometric quantification of the blots after normalization with GAPDH level. *$P < 0.05$ vs. WT-saline. $^{\#}P < 0.05$ vs. 3xTg-saline. (C) Representative immunohistochemical staining of the frozen tissue sections of the mouse brains (magnification: 20x).

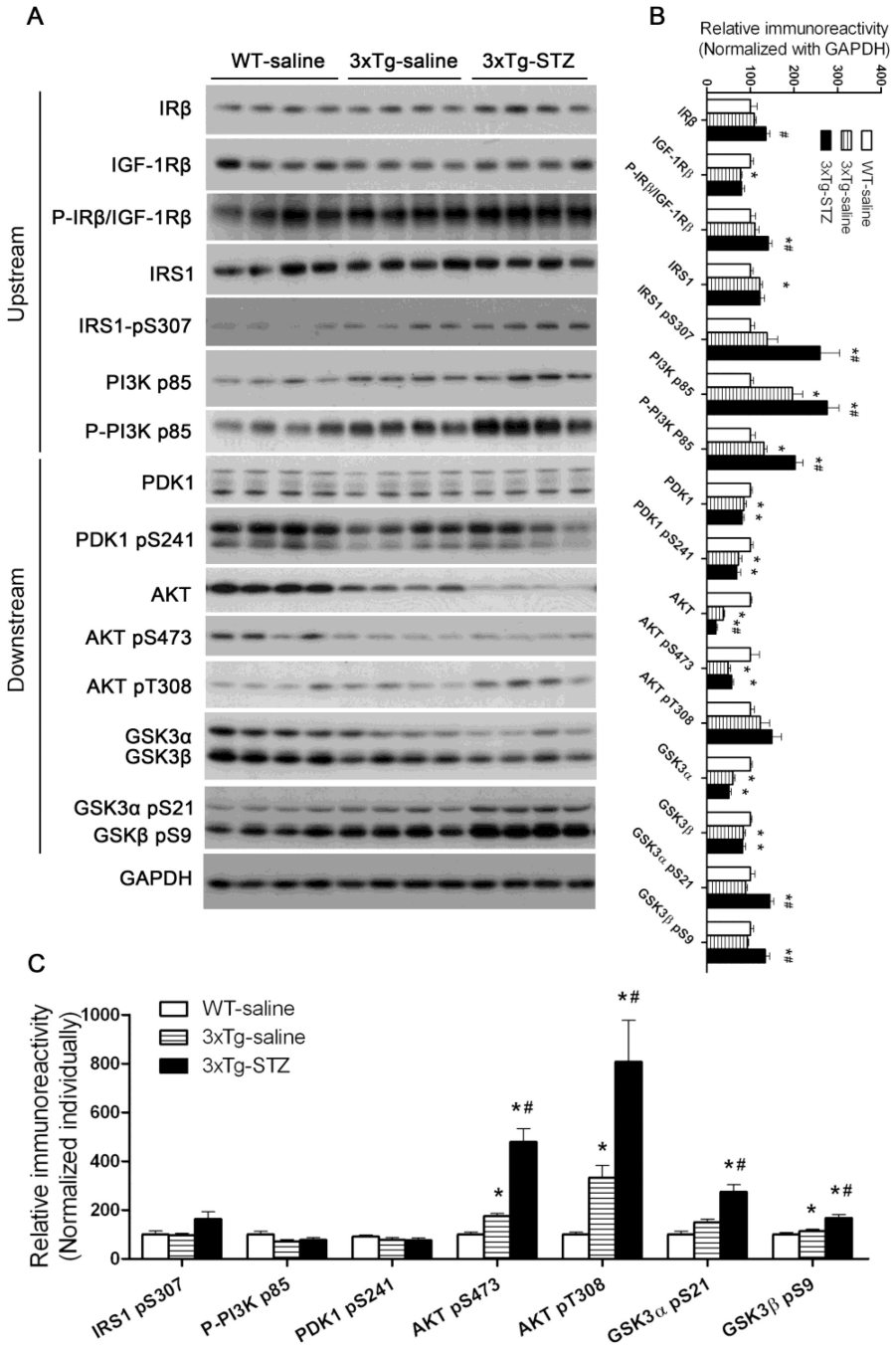

Fig. 7.

Effects of icv STZ on the brain insulin signaling pathway in 3xTg-AD mice. (A) Hippocampal homogenates from WT-saline, 3xTg-saline and 3xTg-STZ mice were analyzed by Western blots developed with antibodies indicated on the left of the blots. (B, C) Densitometrical quantification of the blots after normalization with either the GAPDH level (B) or the corresponding protein level (C). *$p < 0.05$ vs. WT-saline; #$p < 0.05$ vs. 3xTg-saline.

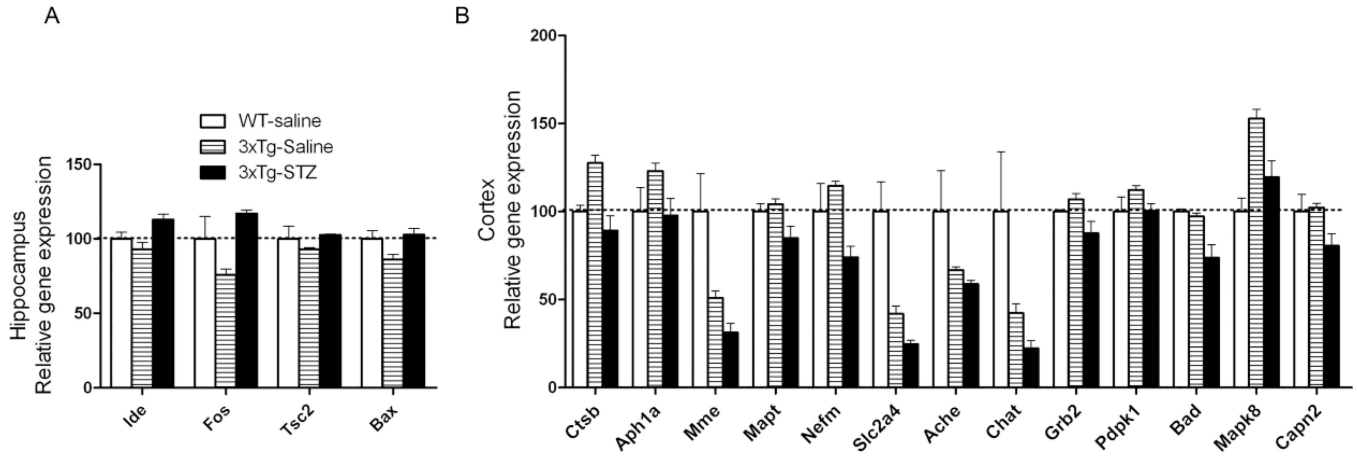

Fig. 8.

Effects of icv STZ on the expression of AD-related genes in the 3xTg-AD mouse brains. Only those genes whose relative expression levels were significantly different ($p < 0.05$) between the 3xTg-saline mice and the 3xTg-STZ mice are shown.

Table 1

Primary antibodies used in this study

Antibody	Type	Specificity	Phosphorylation sites	Source / Reference
GFAP	Mono-	GFAP		Millipore, Temecula, CA, USA
Iba1	Poly-	Iba1		Wako Chemicals, Richmond, VA, USA
Synaptophysin	Mono-	Synaptophysin		Millipore
PSD95	Mono-	PSD95		Cell signaling Technology, Danvers, MA, USA
GluR1	Poly-	GluR1		Millipore
GluR2/3	Mono-	GluR2/3		Abcam, Cambridge, MA, USA
NR1	Poly-	NR1		Thermo Scientific, Pittsburg, PA, USA
IRβ	Poly-	IRβ		Cell signaling Technology
IGF-1Rβ	Poly-	IGF-1Rβ		Cell signaling Technology
P-IRβ/IGF -1Rβ	Mono-	P-IRβ/IGF -1Rβ	Tyr1150/1151(IRβ), Tyr1135 /1136 (IGF-1Rβ)	Cell signaling Technology
IRS1	Poly-	IRS1		Cell signaling Technology
IRS1 pS307	Poly-	P-IRS1	Ser307	Cell Signaling Technology
PI3K p85	Poly-	PI3K (p85)		Cell Signaling Technology
P-PI3K p85	Poly-	P-PI3K (p85)	Tyr458/Tyr199	Cell Signaling Technology
PDK1	Poly-	PDK1		Cell Signaling Technology
PDK1 pS241	Poly-	P-PDK1	Ser241	Cell Signaling Technology
AKT	Poly-	AKT		Cell Signaling Technology
AKT pS473	Poly-	P-AKT	Ser473	Cell Signaling Technology
AKT pT308	Poly-	P-AKT	Thr308	Cell Signaling Technology
GSK-3α/β pS21/9	Poly-	P-GSK-3α/β	Ser21/9	Cell Signaling Technology
GSK-3α/β	Poly-	GSK-3β		Cell Signaling Technology
R134d	Poly-	Tau		[70]
pS199/202	Poly-	P-tau	Ser199/2002	Invitrogen, Grand Island, NY, USA
pT205	Poly-	P-tau	Thr205	Invitrogen
pT212	Poly-	P-tau	Thr212	Invitrogen
pS214	Poly-	P-tau	Ser214	Invitrogen
pT231	Poly-	P-tau	Thr231	Invitrogen
12E8	Mono-	P-tau	Ser262/356	Dr. D. Schenk
PHF-1	Mono-	P-tau	Ser396/404	Dr. P. Davies
pS404	Poly-	P-tau	Ser404	Invitrogen
pS422 (R145)	Poly-	P-tau	Ser422	[71]
Anti-GAPDH	Poly-	GAPDH		Santa Cruz Biotechnology
6E10	Mono-	APP and Aβ		Covance, Princeton, NJ, USA